Observation of electromagnetically induced Talbot effect in an atomic system

Zhaoyang Zhang,[1,2] Xing Liu,[2] Dan Zhang,[1,2] Jiteng Sheng,[3] Yiqi Zhang,[2] Yanpeng Zhang,[2,*] and Min Xiao[1,4,†]

[1]*Department of Physics, University of Arkansas, Fayetteville, Arkansas, 72701, USA*

[2]*Key Laboratory for Physical Electronics and Devices of the Ministry of Education & Shaanxi Key Lab of Information Photonic Technique, Xi'an Jiaotong University, Xi'an, 710049, China*

[3]*State Key Laboratory of Precision Spectroscopy, East China Normal University, Shanghai, 200062, China*

[4]*National Laboratory of Solid State Microstructures and School of Physics, Nanjing University, Nanjing 210093, China*

(Received 6 April 2017; revised manuscript received 23 June 2017; published 3 January 2018)

The electromagnetically induced Talbot effect (EITE) resulting from the repeated self-reconstruction of a spatially intensity-modulated probe field is experimentally demonstrated in a three-level atomic configuration. The probe beam is launched into an optically induced lattice (established by the interference of two coupling fields) inside a rubidium vapor cell and is diffracted by the electromagnetically induced grating that was formed. The diffraction pattern repeats itself at the planes of integer multiple Talbot lengths. In addition, a fractional EITE is also investigated. The experimental observations agree well with the theoretical predictions. This investigation may potentially pave the way for studying the nonlinear and quantum dynamical features that have been predicted for established periodic optical systems.

DOI: 10.1103/PhysRevA.97.013603

The Talbot effect is a self-imaging or lensless imaging phenomenon that was first implemented by launching very weak white light into a Fraunhofer diffraction grating and observing the images of the same periodic structure at certain distances, which were integer multiples of the so-called Talbot length [1,2]. Due to its wide practicability and simplicity [3], research on the Talbot effect has extended to various topics, such as optical measurements [4], optical computing [5], waveguide arrays [6], parity-time symmetric optics [7], x rays [8], Bose-Einstein condensates [9], second-harmonic generation [10], exciton polaritons [11], far-field diffraction regimes [12], and self-accelerating beams [13,14].

Recently, due to the coherent nature and multiparameter tunability of atoms, promising results related to self-imaging in atomic media have been investigated using different techniques, such as matter waves [15–21], atomic density gratings [22], noise-induced energy resonance [23], and entangled photon pairs [24]. In 2011, the Talbot effect based on an electromagnetically induced grating (EIG) [25] was theoretically proposed in a multilevel ultracold atomic medium [26]. This electromagnetically induced Talbot effect (EITE), which is assisted by electromagnetically induced transparency (EIT) [27], can possess certain distinguishable features due to the light-induced atomic coherence in atomic media. First, the Talbot effect is generally considered as a self-imaging method. The EITE can be potentially developed into an attractive alternative for directly observing ultracold atoms or molecules in a cloud. The generation of the EITE in an atomic cloud does not alter the original atomic density distribution. Essentially, under the EIT condition, the near-resonant absorption of the medium is significantly reduced within a certain frequency width (the EIT window) of the probe field under the action of a coherent coupling field on a linked transition [27]. Second, considering that the EITE results from the transmission of light, it can reveal the inhomogeneous density of an atomic sample. Third, the induced EIG can be an amplitude, phase, or a hybrid of amplitude and phase simply by adjusting the corresponding experimental parameters [25]; thus the Talbot effects resulting from different types of gratings can lead to various applications.

In a multilevel EIT atomic configuration, in addition to modifying the linear absorption and dispersion properties of the probe field, the atomic coherence induced by the coupling and probe beams can significantly enhance the Kerr-nonlinear index of refraction near the two-photon atomic resonance [28,29]. Such enhanced near-resonant nonlinearity produces certain unavoidable effects during the self-imaging process and must be taken into account. Even the sign of the modified Kerr-nonlinear coefficient n_2 changes if the sign of the coupling or probe frequency detuning is altered. Such a sign reversal certainly changes the total refractive index, $n = n_0 + n_2 I_c$ (where n_0 and I_c are defined as the linear refractive index and the coupling beam intensity, respectively), and it can be used to balance the linear dispersion [30,31], which implies that frequency detunings of the laser beams can modify the spatially periodical refractive index during the self-imaging process.

In this paper, we experimentally demonstrate the EITE effect as a potential imaging tool by forming an EIG under an EIT condition in a three-level ^{85}Rb atomic medium. The induced optical lattice (i.e., the EIG) inside the atomic vapor cell is established by the interference of a pair of coupling laser beams, and a probe field is launched into it. As a result, a spatially intensity-modulated probe field [32] can be obtained at the output plane of the vapor cell, reflecting the formation of the spatially modulated susceptibility inside the

*ypzhang@mail.xjtu.edu.cn
†mxiao@uark.edu

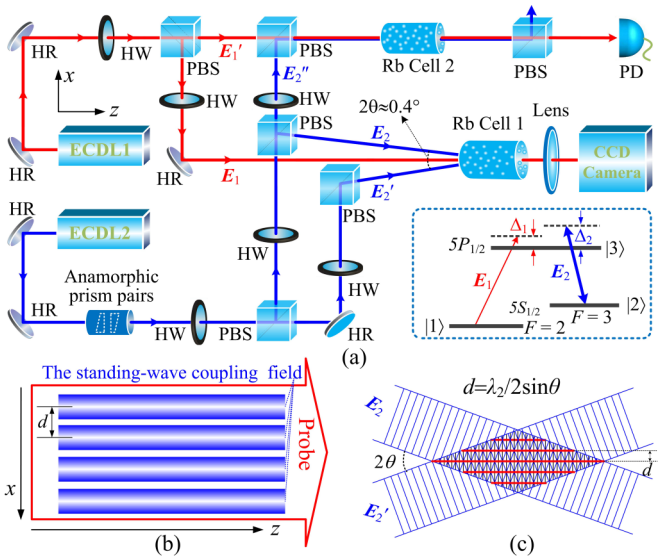

FIG. 1. (a) Experimental setup and the Λ-type energy-level configuration (in the dashed box). The probe beam $\boldsymbol{E}_1$ is imaged onto a CCD camera with a lens. Beams $\boldsymbol{E}_1'$ and $\boldsymbol{E}_2''$ are injected into the auxiliary cell 2 to generate an EIT window in the frequency domain to calibrate the frequencies of the lasers. ECDL: external cavity diode laser, HW: half-wave plate, HR: high-reflectivity mirror, PBS: polarization beam splitter, PD: photodiode detector. (b) The spatial arrangements of the coupling (blue) and probe (red) fields inside the medium to form an EIG. (c) Schematic of the interfering wave front of the two coupling fields $\boldsymbol{E}_2$ and $\boldsymbol{E}_2'$.

atomic medium. The EIT-assisted Talbot effect (or EITE) is manifested through the repeated recurrence of the periodically modulated probe field at certain propagation distances. The experimentally measured axially repeated period agrees well with the theoretical Talbot length d^2/λ_1 [26], where d and λ_1 are defined as the spatial period of the optical lattice and wavelength of the probe field, respectively. Although the current work is implemented in an atomic vapor cell, this effect will certainly work better in ultracold atoms where the Doppler effect is negligible.

The experimental setup and relevant energy-level structure are shown in Fig. 1(a). The probe field $\boldsymbol{E}_1$ (wavelength $\lambda_1 = 794.97$ nm, frequency ω_1, horizontal polarization, and Rabi frequency Ω_1) copropagates with two elliptically shaped coupling beams to interact with the Λ-type ^{85}Rb atoms [the energy-level structure is given in the dashed box of Fig. 1(a)]. The atomic system includes two hyperfine states, $F = 2$ (state $|1\rangle$) and $F = 3$ (state $|2\rangle$), of the ground state $5S_{1/2}$ and one excited state $5P_{1/2}$ (state $|3\rangle$). Two coupling beams, $\boldsymbol{E}_2$ and $\boldsymbol{E}_2'$ ($\lambda_2 = 794.97$ nm, ω_2, vertical polarization, and Ω_2 and Ω_2', respectively) from a single-mode tunable external cavity diode laser (ECDL2) are symmetrically arranged with respect to the z direction. They intersect at the center of Rb cell 1 with an angle of $2\theta \approx 0.4^\circ$ to construct an optically induced lattice along the transverse direction x when the frequency detuning Δ_2 is tuned to be in near resonance with the transition $|1\rangle \rightarrow |2\rangle$. Here, $\Delta_i = \omega_{ij} - \omega_i$ is the detuning between the atomic resonant frequency ω_{ij} ($j = 1,2,3$) and the laser frequency ω_i of $\boldsymbol{E}_i$ ($i = 1,2$). The 7.5-cm-long cell 1 is wrapped with μ-metal sheets to shield the magnetic field and heated by a heat tape to provide an atomic density of $\sim 2.0 \times 10^{12}\,\mathrm{cm}^{-3}$ at 80 °C. The spatial periodicity of the optical lattice was calculated to be $d = \lambda_2/2\sin\theta \approx 114\,\mu$m. Realizing such an EIG is widely believed to be quite challenging in an inhomogeneous Doppler-broadening medium due to the ballistic or diffusive behaviors of moving thermal atoms. Consequently, we adopt this small-angle paraxial arrangement to suppress the severe Doppler effect.

When the weak probe beam $\boldsymbol{E}_1$, which has an elliptical-Gaussian profile (from ECDL1), is launched into the induced lattice, it experiences a spatially modulated index of refraction during propagation under the EIT condition [32,33]. Figure 1(b) shows the spatial arrangements of the laser beams inside the atomic medium for forming an EIG, and the schematic of the interfering wave front of the two coupling fields is shown in Fig. 1(c). By carefully choosing the parameters such as frequency detuning and the Rabi frequencies of the probe and coupling fields, clear diffracted probe beam patterns from the EIG can be observed at the output plane of the cell, which is monitored by a charge-coupled device (CCD) camera equipped with an imaging lens. The Rabi frequency is defined as $\Omega_i = \mu_{ij}E_i/\hbar$ for the transition $|i\rangle \leftrightarrow |j\rangle$, where μ_{ij} is the dipole momentum, and E_i is the electric-field amplitude of beam $\boldsymbol{E}_i$. The behaviors of the probe field during the propagation out of the cell are imaged onto the CCD camera by moving the lens (placed on a precision translation stage) along the z direction. Meanwhile, the CCD camera (fixed on another translation stage) is also moved to maintain the distance between the camera and the lens (along the z direction) to be twice the lens's focal length, which guarantees consistency in the imaging results at different observing planes. In addition, we use an EIT window to calibrate the frequencies of the $\boldsymbol{E}_1$ and $\boldsymbol{E}_2$ fields on the $D1$ transition line [27], which is realized by coupling two beams, $\boldsymbol{E}_1'$ and $\boldsymbol{E}_2''$ (from the above-mentioned ECDL1 and ECDL2, respectively), into a second auxiliary cell 2 to generate the Λ-type EIT spectrum for reference.

The key point of the experiment is to periodically modulate the refractive index experienced by the probe field. With the EIT condition satisfied, the atomic medium modifies the amplitude of the probe field, which behaves the same way as an amplitude grating exerting modulation on an electromagnetic wave (referred to as an EIG effect). Correspondingly, the Kerr-nonlinear coefficient, expressed as $n_2 \propto \mathrm{Re}[\chi^{(3)}]$ [28], is also inevitably enhanced and modified when forming the EIG. As a result, the susceptibility [defined as $\chi = (2N\mu_{31}/\varepsilon_0 E_1)\rho_{31}$ between states $|1\rangle$ and $|3\rangle$ is given by $\chi = \chi^{(1)} + \chi^{(3)}(|\Omega_2|^2 + |\Omega'_2|^2)$, where the linear ($\chi^{(1)}$) and nonlinear ($\chi^{(3)}$) susceptibilities are expressed as [28]

$$\chi^{(1)} = \frac{iN|\mu_{31}|^2}{\hbar\varepsilon_0}\frac{1}{\Gamma_{31} + i\Delta_1 + \frac{|\Omega_2|^2+|\Omega'_2|^2+2\Omega_2\Omega'_2\cos(2k_2x)}{\Gamma_{21}+i\Delta_2}}, \tag{1}$$

and

$$\chi^{(3)} = \frac{-iN|\mu_{31}|^2}{\hbar\varepsilon_0} \frac{1}{\left[\Gamma_{31} + i\Delta_1 + \frac{|\Omega_2|^2+|\Omega'_2|^2+2\Omega_2\Omega'_2\cos(2k_2x)}{\Gamma_{21}+i\Delta_2}\right](\Gamma_{21}+i\Delta_2)}. \quad (2)$$

In the above expressions, $\Gamma_{ij} = (\Gamma_i + \Gamma_j)/2$ is the decay rate between states $|i\rangle$ and $|j\rangle$; Γ_i is the transverse relaxation rate determined by the longitudinal and reversible transverse relaxation times; N is the atomic density at the ground state $|1\rangle$. Furthermore, by adopting the plane-wave expansion method, the one-dimensional periodically modulated total refractive index [34,35] can be approximately described as

$$n(x) \approx n_0 + \Delta n_1 \cos(2k_2x) + \Delta n_2 \cos(4k_2x), \quad (3)$$

where n_0 is the uniform refractive index independent of the spatial periodicity; Δn_1 and Δn_2 are coefficients with different spatial periodicities for spatially varying terms in the total refractive indices; n_0 contains the linear and periodicity-independent parts contributed by $\chi^{(1)}$ and $\chi^{(3)}$, both of which also contribute to Δn_1; term $\Delta n_2 \cos(4k_2x)$ accounts for the nonlinear index. Equation (3) shows a physical picture of the spatially modulated refractive index in the presence of a standing-wave coupling field in a three-level EIT medium. In fact, the spatial distribution of the total refractive index can be shifted or modulated along the transverse direction of x under certain parameters, which can be viewed as a result of the balance between the linear and nonlinear refractive indices. To precisely show the EITE with nonlinearity, numerical simulations are performed based on a previous proposal [26], and details are provided in the Supplemental Material [36]. As a result, the probe transmission at distances of mZ_T ($Z_T = d^2/\lambda_1$ is the Talbot length, and positive integer m is the self-imaging number) can repeat its amplitude pattern at the output plane of the cell with (for odd m) and without (for even m) shifting a half period. The parameters used in the experiment result in a Talbot length of $Z_T \approx 16.3$ mm, which is quite long due to the relatively long EIG period d.

Furthermore, we can numerically plot the carpet of the EITE, as shown in the Supplemental Material [36]. By comparing the situations with and without considering $\chi^{(3)}$, we find that the Talbot length is the same for both cases, which agrees with the prediction that the Talbot distance is determined only by the periodicity of the induced optical lattice and the probe wavelength. The effects introduced by $\chi^{(3)}$ include that (I) third-order nonlinearity can render a change in the intensity profile of the generated EIG and the intensity of the diffracted probe field near resonance, and (II) $\chi^{(3)}$ can shift the output probe field by a half period along the x direction when Δ_1 is tuned across a certain value, which is not obtained for the linear case.

In the experiment, when the probe beam [see Fig. 2(a)] is launched into the spatially modulated optical lattice, it will be diffracted into a periodic pattern. Figure 2(b) is diffraction pattern of the probe beam after propagating through the optically induced lattice. The one-photon detuning for the probe field and two-photon detuning are set as $\Delta_1 = 100$ MHz and $\Delta_1 - \Delta_2 = -20$ MHz, respectively. When propagating through the atomic medium, the probe beam can be absorbed at $\Delta_1 = 100$ MHz. Since the EIT window is generated under the two-photon Doppler-free condition [37], the Doppler effect plays a less important role here. The generated interference fringe of the two coupling fields is depicted in Fig. 2(c). Figure 2(d) shows the transmission spectra of the probe field from auxiliary Rb cell 2, with the lower and upper curves representing the absorption without and with the EIT window, respectively. Notably, the optical pumping effect [28] exists in this Λ-type system, which increases the absorption of the probe field on the $D1$ line and makes the intensity of the probe transmission at $\Delta_1 - \Delta_2 = 0$ slightly weaker than that with $\boldsymbol{E}_2$ off.

When the EIG-diffracted probe image is observed at the output plane of the cell ($z = 0$), we monitor the propagation characteristics of the intensity-modulated probe beam by simultaneously moving the CCD camera and the imaging lens. The observed images at different z planes (distances) are shown in Figs. 3(a1)–3(a9). The experimental results show that the diffracted image shifts by a half period (compared to that at $z = 0$) when the observation plane is set to $z \approx 15$ mm, which basically agrees with the theoretically predicted Talbot length of $Z_T = 16.3$ mm. The error between the theoretical prediction and the experimental observation is possibly introduced by the uncertainty in estimating the beam intersection angle, which is too small to be precisely measured. When the observation distance exceeds $z = 15$ mm (the first Talbot plane), the diffracted image gradually shifts back (along the

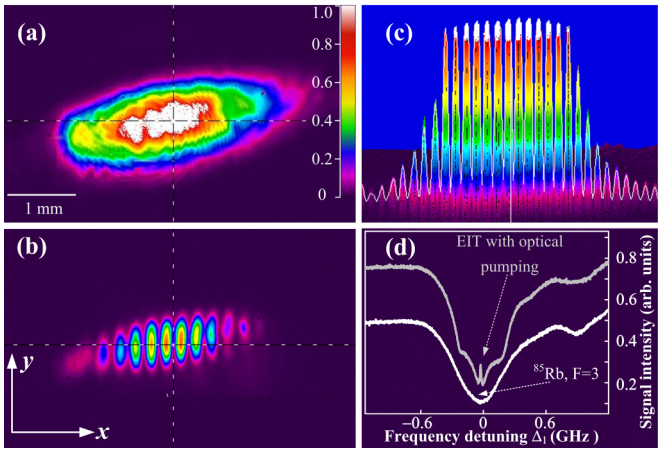

FIG. 2. (a) Image of the probe beam. The cross dashed line is from the control software for the CCD camera. During the experiment, the cross line is fixed to denote a reference point, and based on this point one can recognize the spatial shift of the output probe beam. (b) Generated diffraction pattern of the probe field. (c) Observed three-dimensional view interference fringe of the two coupling beams. (d) Reference EIT signal. The upper and lower curves are the EIT signal and the absorption spectrum corresponding to the transition of ^{85}Rb, $F = 3 \rightarrow F'$, respectively. (b,c) share the same color bar as (a). The units of the color bar are mW.

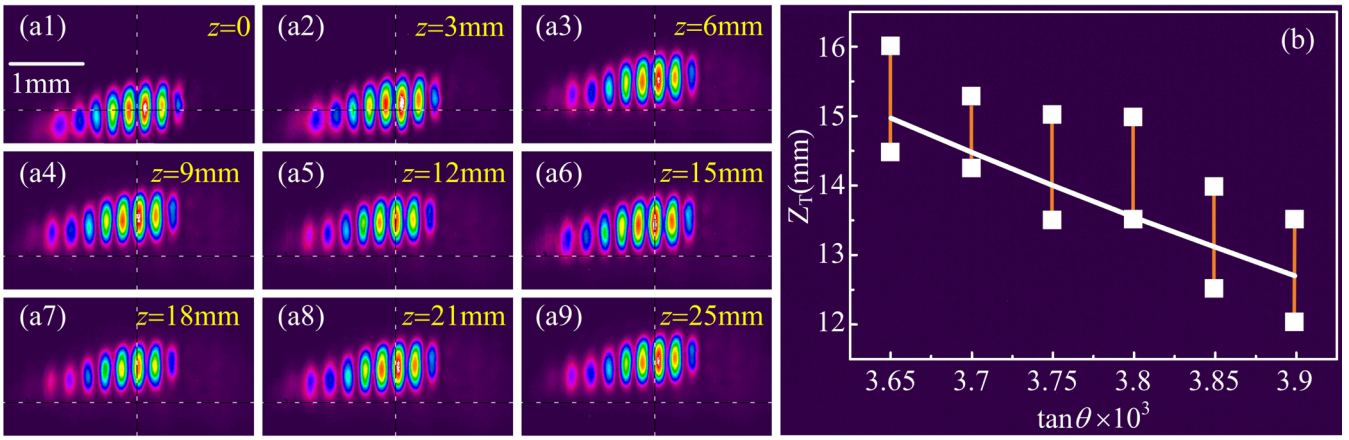

FIG. 3. Demonstration of the electromagnetically induced Talbot effect. (a) Images of the probe field at different distances. (b) Dependence of the Talbot length on the angle θ. The squares are the experimental observations, and the solid curve is the theoretical prediction.

opposite direction of the movement towards the $m = 1$ plane) to recover the image at $z = 0$. Due to the limitation of the precision translation stage's maximum displacement (25 mm), the image at the second Talbot plane ($m = 2$) could not be captured in our current experiment. However, the moving trend of the images at $z = 18$, 21, and 25 mm indicates that the image at approximately $z \approx 30$ mm should recover the image at the output surface of the cell. The experimentally observed images at the first (m is an odd integer) and second (m is an even integer) Talbot planes support the theoretical predictions. Additionally, Fig. 3(b) shows the experimentally measured evolution of the Talbot length with the change in angle 2θ, which affects the periodicity of the interference fringe in the medium. For a given angle 2θ, two measured values exist (maximum and minimum values), showing a range in which the recurrence effect seems to be optimal. Namely, in this range (the distance between the minimum and maximum z values), the observed images are almost unchanged with z and the accurate Talbot length will fall in this marked range. The experimental results agree well with the theoretical prediction (solid curve), which indicates that the Talbot length can be controlled by the period of the induced optical lattice. When working with small ultracold atomic samples, one can easily increase the angle 2θ to reduce the EIG period d since no Doppler effect needs to be considered. The trade-off for decreasing d is a reduction in the Talbot length Z_T, which can be practically compensated for by using a simple imaging lens, as we have done in the current experiment.

Furthermore, fractional EITE is also observed in our experiment, as shown in Fig. 4. The periodicity of the diffraction patterns at $z = Z_T/2$ and $z = 3Z_T/2$ is doubled. Based on the measured integer Talbot effect, the Talbot length, Z_T, is approximately 15 mm. The periodicity-doubled images are observed at approximately $z = 8$ mm ($\approx Z_T/2$) and $z = 22$ mm ($\approx 3Z_T/2$), which agree well with the calculated fractional Talbot length.

Lastly, we provide evidence for the existence of nonlinearity in this self-imaging process. Kerr-type nonlinearity in the atomic medium is verified by observing a spatial shift (induced by the combined effects of the linear and nonlinear dispersions near the resonance) of the diffracted probe beam. As shown in Fig. 5, with the frequency detuning of the coupling field fixed at $\Delta_2 = 0$, the diffracted pattern varies with two-photon detuning, $\delta = \Delta_1 - \Delta_2$. The periodical probe field has the

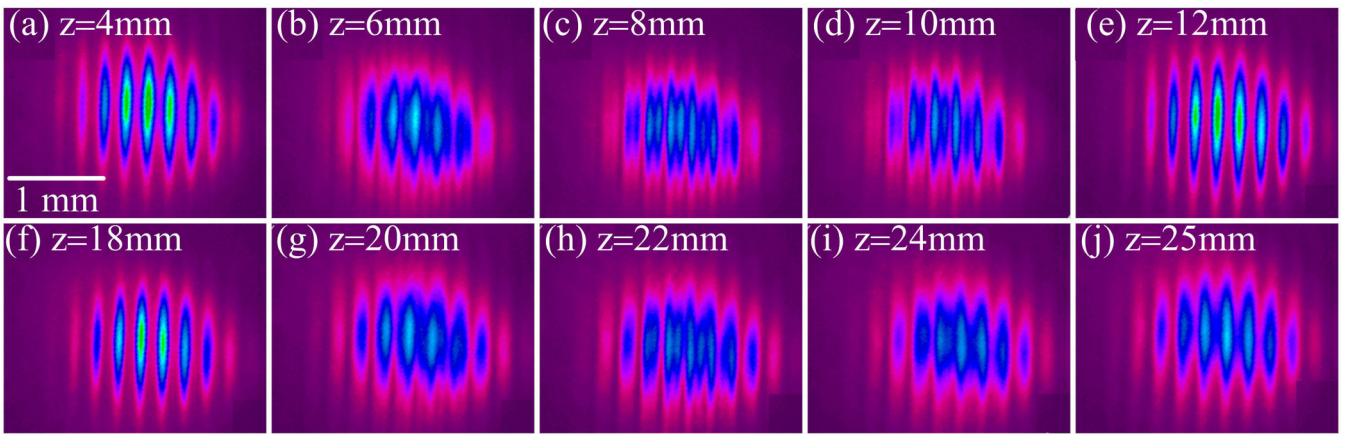

FIG. 4. Observed fractional Talbot effect (double periodicity) at $z = 8$ mm ($\approx Z_T/2$) and $z = 22$ mm ($\approx 3Z_T/2$). The experimentally observed integer Talbot length is $Z_T \approx 15$ mm.

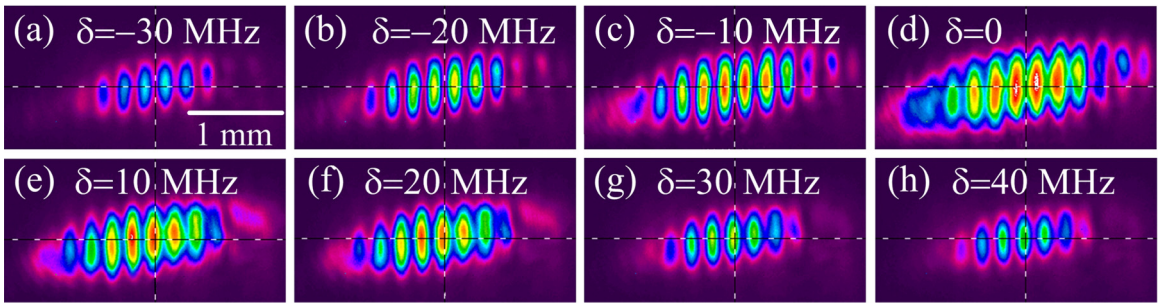

FIG. 5. Observed diffracted probe beam patterns versus two-photon detuning $\delta = \Delta_1 - \Delta_2$. (a) $\delta = -30$ MHz, (b) $\delta = -20$ MHz, (c) $\delta = -10$ MHz, (d) $\delta = 0$, (e) $\delta = 10$ MHz, (f) $\delta = 20$ MHz, (g) $\delta = 30$ MHz, and (h) $\delta = 40$ MHz.

strongest intensity value near the resonance $\delta = 0$, whereas it becomes much weaker at points far away from the resonance ($\delta = -30$ and 40 MHz). Particularly, the diffracted pattern shifts by a distance of $d/2$ along the transverse x direction when the frequency detuning varies from $\Delta_1 = 0$ to $\Delta_1 = 10$ MHz. This observed spatial shift can be attributed to the abrupt sign change (negative $\leftrightarrow$ positive) of n_2 [38]. Specifically, both terms Δn_1 and Δn_2 in Eq. (3) can be manipulated by controlling Δ_1 according to Eqs. (1) and (2). As a result, when Δn_1 and Δn_2 are of the same magnitude level [39] by properly setting the parameters, the total $n(x)$ can shift spatially by a half period when Δ_1 changes from negative to positive. This spatial shift can provide another way to modulate the imaging process in ultracold atomic clouds without modifying the experimental setup. The effects of this spatial shift in the fringe pattern due to modified nonlinearity in a self-imaging process require further exploration.

In summary, the EIT-assisted Talbot effect in a three-level atomic vapor cell is experimentally demonstrated. In principle, this imaging method can certainly be extended to ultracold atomic clouds and Bose-Einstein condensate systems, considering that EIG in the frequency domain has already been experimentally demonstrated in cold sodium atoms under EIT conditions [40]. Considering that the Talbot effect is widely adopted as an imaging technique, this EIG-based self-imaging technique can potentially offer an alternative way to image ultracold gas samples. Additionally, because of the easy controllability of the linear absorption and dispersion properties and the Kerr nonlinearity, this coherently prepared multilevel atomic configuration can be used as an ideal platform to further investigate intriguing nonlinear and quantum beam dynamical features that are predicted for constructed periodic optical systems beyond the EITE. For example, our system can be applied to demonstrate the proposed parity-time-symmetric Talbot effect [7] by adding another standing-wave pump field to construct the parity-time symmetry potential [33] and to explore other interesting physics in induced optical lattices.

We acknowledge helpful discussions with J. M. Wen. This work was supported in part by National Key R&D Program of China (Grant No. 2017YFA0303703), National Natural Science Foundation of China (Grants No. 61605154 and No. 11474228), Key Scientific and Technological Innovation Team of Shaanxi Province (2014KCT-10), Natural Science Foundation of Shaanxi Province (Grants No. 2017JQ6039 and No. 2017JZ019) and China Postdoctoral Science Foundation (Grants No. 2016M600776, No. 2016M600777, and No. 2017T100734).

[1] H. F. Talbot, London, Edinburgh, and Dublin Philos. Mag. J. Sci. **9**, 401 (1836).
[2] L. Rayleigh, Philos. Mag. **11**, 196 (1881).
[3] J. M. Wen, Y. Zhang, and M. Xiao, Adv. Opt. Photonics **5**, 83 (2013).
[4] P. Xi, C. Zhou, E. Dai, and L. Liu, Opt. Express **10**, 1099 (2002).
[5] K. Patorski, Prog. Opt. **27**, 1 (1989).
[6] R. Iwanow, D. A. May-Arrioja, D. N. Christodoulides, G. I. Stegeman, Y. Min, and W. Sohler, Phys. Rev. Lett. **95**, 053902 (2005).
[7] H. Ramezani, D. N. Christodoulides, V. Kovanis, I. Vitebskiy, and T. Kottos, Phys. Rev. Lett. **109**, 033902 (2012).
[8] F. Pfeiffer, M. Bech, O. Bunk, P. Kraft, E. F. Eikenberry, Ch. Brönnimann, C. Grünzweig, and C. David, Nat. Mater. **7**, 134 (2008).
[9] C. Ryu, M. F. Andersen, A. Vaziri, M. B. d'Arcy, J. M. Grossman, K. Helmerson, and W. D. Phillips, Phys. Rev. Lett. **96**, 160403 (2006).
[10] Y. Zhang, J. M. Wen, S. N. Zhu, and M. Xiao, Phys. Rev. Lett. **104**, 183901 (2010).
[11] T. Gao, E. Estrecho, G. Li, O. A. Egorov, X. Ma, K. Winkler, M. Kamp, C. Schneider, S. Höfling, A. G. Truscott, and E. A. Ostrovskaya, Phys. Rev. Lett. **117**, 097403 (2016).
[12] J. Azaña and H. Guillet de Chatellus, Phys. Rev. Lett. **112**, 213902 (2014).
[13] Y. Lumer, L. Drori, Y. Hazan, and M. Segev, Phys. Rev. Lett. **115**, 013901 (2015).
[14] Y. Zhang, H. Zhong, M. R. Belić, X. Liu, W. Zhong, Y. Zhang, and M. Xiao, Opt. Lett. **40**, 5742 (2015).
[15] K. Li, L. Deng, E. W. Hagley, M. G. Payne, and M. S. Zhan, Phys. Rev. Lett. **101**, 250401 (2008).
[16] J. F. Clauser and S. Li, Phys. Rev. A **49**, R2213(R) (1994).
[17] M. S. Chapman, C. R. Ekstrom, T. D. Hammond, J. Schmiedmayer, B. E. Tannian, S. Wehinger, and D. E. Pritchard, Phys. Rev. A **51**, R14(R) (1995).
[18] S. Nowak, Ch. Kurtsiefer, T. Pfau, and C. David, Opt. Lett. **22**, 1430 (1997).

[19] R. Abfalterer, C. Keller, S. Bernet, M. K. Oberthaler, J. Schmiedmayer, and A. Zeilinger, Phys. Rev. A **56**, R4365(R) (1997).
[20] M. Weitz, T. Heupel, and T. W. Hänsch, EPL **37**, 517 (1997).
[21] L. Deng, E. W. Hagley, J. Denschlag, J. E. Simsarian, M. Edwards, C. W. Clark, K. Helmerson, S. L. Rolston, and W. D. Phillips, Phys. Rev. Lett. **83**, 5407 (1999).
[22] C. Li, T. Zhou, Y. Zhai, X. Yue, J. Xiang, S. Yang, W. Xiong, and X. Chen, Phys. Rev. A **95**, 033821 (2017).
[23] M. Sadgrove, S. Kumar, and K. Nakagawa, Phys. Rev. Lett. **103**, 010403 (2009).
[24] X.-B. Song, H.-B. Wang, J. Xiong, K. Wang, X. Zhang, K.-H. Luo, and L.-A. Wu, Phys. Rev. Lett. **107**, 033902 (2011).
[25] H. Y. Ling, Y. Q. Li, and M. Xiao, Phys. Rev. A **57**, 1338 (1998).
[26] J. M. Wen, S. W. Du, H. Y. Chen, and M. Xiao, Appl. Phys. Lett. **98**, 081108 (2011).
[27] J. Gea-Banacloche, Y. Q. Li, S. Z. Jin, and M. Xiao, Phys. Rev. A **51**, 576 (1995).
[28] H. Wang, D. Goorskey, and M. Xiao, Phys. Rev. Lett. **87**, 073601 (2001).
[29] J. Sheng, X. Yang, H. Wu, and M. Xiao, Phys. Rev. A **84**, 053820 (2011).
[30] H. Wang, D. Goorskey, and M. Xiao, Opt. Lett. **27**, 258 (2002).
[31] H. Wu and M. Xiao, Opt. Lett. **32**, 3122 (2007).
[32] J. Sheng, J. Wang, M.-A. Miri, D. N. Christodoulides, and M. Xiao, Opt. Express **23**, 19777 (2015).
[33] Z. Zhang, Y. Zhang, J. Sheng, L. Yang, M.-A. Miri, D. N. Christodoulides, B. He, Y. Zhang, and M. Xiao, Phys. Rev. Lett. **117**, 123601 (2016).
[34] Y. Zhang, Z. Wang, Z. Nie, C. Li, H. Chen, K. Lu, and M. Xiao, Phys. Rev. Lett. **106**, 093904 (2011).
[35] Y. Zhang, Z. Wang, H. Zheng, C. Yuan, C. Li, K. Lu, and M. Xiao, Phys. Rev. A **82**, 053837 (2010).
[36] See Supplemental Material at http://link.aps.org/supplemental/10.1103/PhysRevA.97.013603 for the theoretical derivation of Talbot length.
[37] Y. Q. Li and M. Xiao, Phys. Rev. A **51**, R2703 (1995).
[38] Y. Zhang, Z. Nie, H. Zheng, C. Li, J. Song, and M. Xiao, Phys. Rev. A **80**, 013835 (2009).
[39] Z. Wu, Y. Zhang, C. Yuan, F. Wen, H. Zheng, Y. Zhang, and M. Xiao, Phys. Rev. A **88**, 063828 (2013).
[40] M. Mitsunaga and N. Imoto, Phys. Rev. A **59**, 4773 (1999).